Materials Advances

ROYAL SOCIETY OF CHEMISTRY

PAPER

View Article Online
View Journal | View Issue

Cite this: *Mater. Adv.*, 2024, 5, 6205

Effect of fullerene doping on electronic and photovoltaic properties of the cubic bicontinuous phase

Ahmad Murad,[a] Mohamed Alaasar,†*[c] Ahmed F. Darweesh[b] and Alexey Eremin †*[a]

Received 22nd April 2024,
Accepted 25th June 2024

DOI: 10.1039/d4ma00418c

rsc.li/materials-advances

We explored the electrical conductivity and photovoltaic properties of a complex polycatenar liquid crystal that contains a 5,5′-diphenyl-2,2′-bithiophene core and exhibits a nanostructured cubic bicontinuous phase. Owing to their three-dimensional network structures, such materials give rise to continuous conduction channels in three dimensions, minimising the distortions induced by structural defects observed in other liquid crystal phases. Although the pure material doesn't show any photovoltaic behaviour, we found that doping it with fullerenes significantly increases the photocurrent. We also examined the electrical conductivity and charge mobility in the hybrid compound.

1 Introduction

Nanostructured liquid crystalline materials (LCs) offer a promising avenue to create innovative functional materials with unique properties and potential applications.[1] An important class of such LCs are those derived from self-organised π-conjugated systems,[2–4] which have been applied, for example, in thin-film transistors[5–7] and photovoltaic cells.[8] During the last decade, the nanostructured bicontinuous cubic (Cub_{bi}) LC phases formed by π-conjugated rod-like molecules have attracted particular interest[9–17] because of their three-dimensional network structures, giving rise to continuous conduction channels in three dimensions. This unique structure minimizes the distortions induced by structural defects observed in other LC phases.[3]

The majority of recently reported Cub_{bi} phases are exhibited by polycatenar molecules having an unsymmetrical distribution of terminal chains at both ends of the extended aromatic rod-like backbone.[9–16] One of the core units used in designing such Cub_{bi} phases to be applied as semiconductors or photovoltaic cells is the π-conjugated 5,5′-diphenyl-2,2′-bithiophene core.[15,16,18,19] In almost all of these materials, two types of Cub_{bi} phases with different symmetries were reported to differ in the number of the three-way junctions helical networks forming the cubic phase.

In the first type, two networks of opposite chirality sense are involved, leading to the achiral double gyroid phase with space group $Ia\bar{3}d$ ($Cub_{bi}/Ia\bar{3}d$) (see Fig. 1b).[9] On the other hand, the second type is a chiral one composed of three helical networks with a space group $I23$ ($Cub_{bi}^{[*]}/I23$, Fig. 1a).[12] Chirality was even observed in the isotropic phase ($Iso_{I}^{[*]}$) exhibited by some of these polycatenars.[7,9,19,20]

Recently, we reported the design and synthesis of LC polycatenars derived from the π-conjugated rod-like 5,5′-diphenyl-2,2′-dithiophene unit, in which one end has three alkoxy chains, and the other end has one variable thioalkyl chain (compounds Am/n, Fig. 2).[15]

Self-assembly behaviour in these materials was investigated in detail. They were found to exhibit Cub_{bi} phases in extensive temperature ranges >200 K, which in some cases are stable at room temperature, making them excellent candidates for technological applications. Depending on the length of the thioalkyl chain, the two different types of the Cub_{bi} phases, either $Cub_{bi}/Ia\bar{3}d$ or $Cub_{bi}^{[*]}/I23$ were observed in addition to the $Iso_{I}^{[*]}$ phase and tetragonal phase in some derivatives.[14]

This paper investigates the electrical conductivity, photovoltaic properties, and charge mobility in a complex polycatenar liquid crystal containing a 5,5′-diphenyl-2,2′-bithiophene core and exhibiting the cubic bicontinuous phase. Although the pure material does not show any photovoltaic behaviour, we find that doping it with fullerenes significantly increases the photocurrent already at a concentration as low as 2 wt%. Molecular doping using chiral and electronically active acceptor/donor dopants enables the tuning of materials optical, mechanical, and electronic properties. This extends beyond liquid crystal systems to include organic semiconductors,

[a] *Institute of Physics, Otto von Guericke University, 39106 Magdeburg, Germany. E-mail: alexey.eremin@ovgu.de; Tel: +49 391 6750099*
[b] *Dept. of Chemistry, Faculty of Science, Cairo University, Giza, Egypt*
[c] *Martin Luther University, Halle-Wittenberg Kurt Mothes Str. 2, 06120 Halle (Saale), Germany. E-mail: mohamed.alaasar@chemie.uni-halle.de*
† These authors contributed equally to this work.

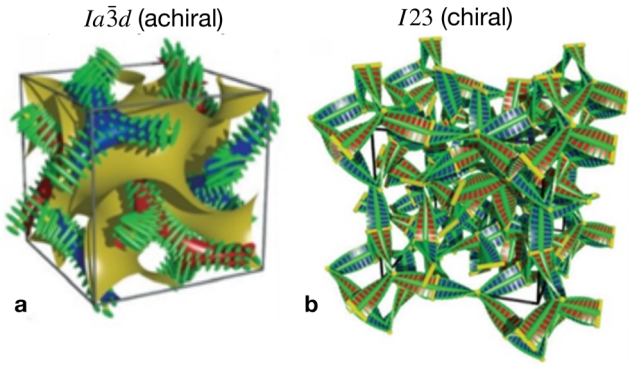

Fig. 1 The two different types of helical network structures of the Cub_{bi} phases exhibited by the nonsymmetric polycatenars (a) the achiral double-gyroid $Cub_{bi}/Ia\bar{3}d$ phase and (b) the chiral $Cub_{bi}^{[*]}/I23$ phase, reproduced from ref. 20 by permission from Wiley.

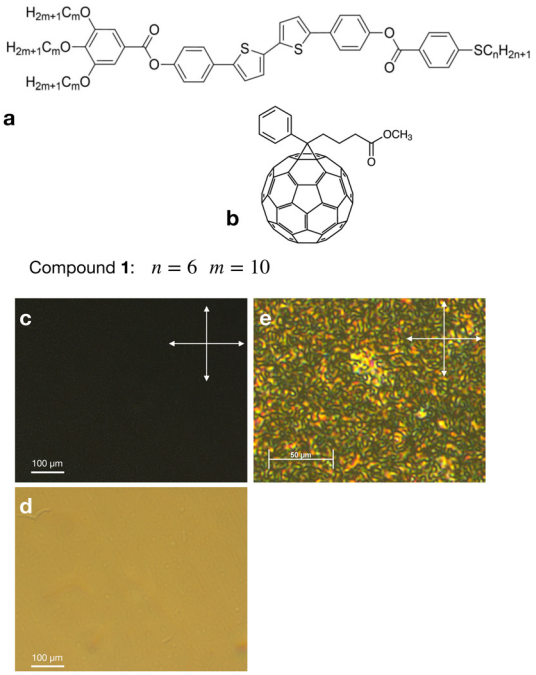

Fig. 2 (a) The chemical structure of the investigated compound, (b) chemical structure of the fullerene dopant. Microscopy images with crossed polarisers (c) and without polarisers (d) in S_2 mixtures at T= 150 °C. (e) Grainy texture (polarising microscopy) of disclination lines observed at room temperature in S_2.

photoluminescent materials, and photochemical and catalytic systems.[21–26]

2 Experimental

2.1 Materials

We studied the photovoltaic effect of the rod-like achiral polycatenar molecules derived from a π-conjugated 5,5′-diphenyl-2,2′-bithiophene core with a fork-like triple alkoxylated end and a variable single alkylthio chain at the other end (Fig. 2), and phenyl-C61-butyric acid methyl ester (PCBM) at different concentration. The synthesis of the compound is described in.[15] As a representative example we selected compound **1** with n = 6 and m = 10 for our study.

Table 1 Chemical composition of the investigated mixtures

Sample	S_1	S_2	S_3	S_4
Concentration of PCPM (mol%)	2.0	4.5	8.7	10.8

The phase transition of compound **1** is as the following: heating: Cr 116 °C [40.6] $Cub_{bi}^{[*]}/I23$ 190 °C [2.5] Iso cooling: Iso 187 °C [<0.1] $Iso_I^{[*]}$ 182 °C [1.9] $Cub_{bi}^{[*]}/I23$ 57 °C [22.2] Cr.

The numbers in brackets provide the transition enthalpies in kJ mol^{-1}. The designations Cr, $Cub_{bi}^{[*]}/I23$ and Iso correspond to the crystalline, cubic bicontinuous and isotropic phases, respectively. The structure of the phase is shown in Fig. 1.

As a dopant, we used [6,6]-phenyl C61 butyric acid methyl ester purchased from Merck. Four mixtures were investigated as listed in Table 1.

2.2 Methods

Optical characterisation of the liquid crystal phases was made using AxioScope Pol and AxioImager polarising microscopes equipped with heat stages (Linkam LTS420 and Instec FS1). The liquid crystal material was filled in a sandwich cell with ITO electrodes (E.H.C. Corp., Japan). The cells with thicknesses 5 and 10 μm were used.

We used a Keithley source meter 2635B (SMU) to perform the conductivity measurements and the characterisation of the photovoltaic effect. The software Kickstart (Keithley) was used to control the SMU. To avoid the relatively high hysteresis of the measured dark current, we opted for a pulsed measuring mode with a dwelling time of 15 seconds between the measuring pulses.

The tungsten light source was used to illuminate and measure the photocurrent, while a Newport Corp. power meter 918D-UV-OD3R was used to measure the light power.

Time-of-flight measurements were made using Q-switched sapphire PDSS laser Helios (Coherent, Germany) at λ = 532 nm, pulse width τ < 690 ps, and the pulse energy 20 μJ. For the signal acquisition, we used a broadband oscilloscope Tektronix 3032b (Tektronix, USA).

3 Results and discussion

Semiconducting liquid crystals are distinguished by a high degree of π-stacking between adjacent molecules, which allows for the carrier transport mechanism to occur.[27] However, disorder in the liquid state can limit this process. Furthermore, ionic impurities can contribute significantly to the material's conductivity. The figure shown in Fig. 3a displays a typical J–V characteristic of the compound being studied. The material's conductivity increases notably with rising temperature, but this

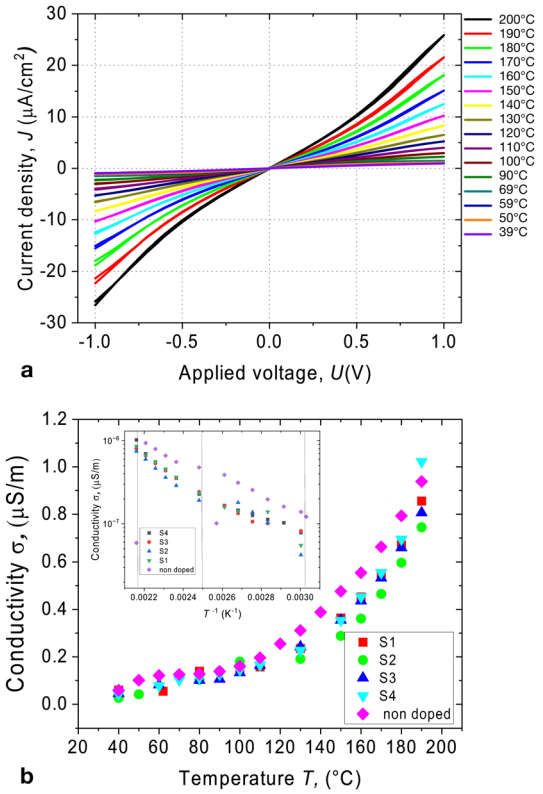

Fig. 3 (a) The current–voltage characteristic at different temperature of compound **1**. (b) The temperature dependence of conductivity for the pure compound and the mixtures. The inset shows the Arrhenius plot of σ. The measurements were made on non-illuminated samples.

is attributed to the reduction of viscosity, which leads to an increase in ionic mobility.

In the crystalline phase, however, the J–V characteristic has a saturating behaviour in sufficiently high fields exhibiting non-linearities. Nevertheless, ohmic behaviour was observed in all phases in the voltage range below 0.5 V. The electric conductivity is weakly temperature-dependent below 100 °C and increases continuously with increasing temperature (Fig. 3b). This growth can be attributed to the thermal activation of the charge transfer mechanism and increasing role of the ionic transport facilitated by the decrease in viscosity. The pure compound behaves as an insulator due to the deficiency of charge carriers and shows no photovoltaic response in the visible spectral range.

In order to solve the problem, we introduced fullerene as a dopant which acts as an electron acceptor (as shown in Fig. 2b). Fullerene is a commonly used material in organic semiconductors due to its bandgap of 1.5 eV.[8,28–30] This property makes it suitable for applications in electronics and photovoltaics. We prepared four different mixtures with varying concentrations of the dopant, which are listed in Table 1.

Admixing such a small amount of C61 dopant to the liquid crystal does not significantly affect the dark current. Fig. 3b shows the temperature dependence of the conductivity under dark conditions. The dark current exhibited a strong temperature dependence, increasing with increasing temperature. No aggregation of fullerenes was observed in the mixture S_1, as was examined using polarising microscopy (see Fig. 2c–e). The cubic phases have optically isotropic texture and appear dark

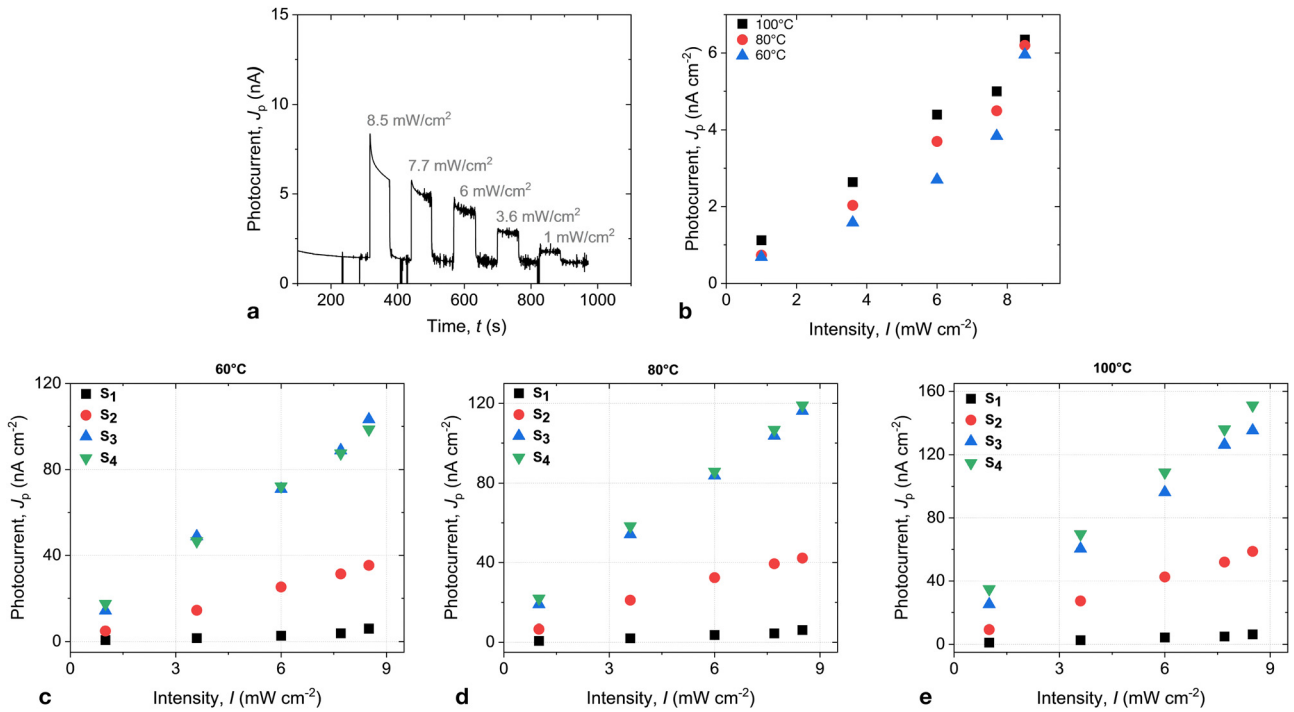

Fig. 4 (a) Exemplary photocurrent recorded in mixture S_1 measured at different light intensities at T = 60 °C und applied voltage U = 1 V. (b) Intensity dependence of the photocurrent measured at U = 1 V. Intensity dependence of the photocurrent in mixtures containing various amounts of C61: at (c) T = 60 °C, (d) T = 80 °C, (e) T = 100 °C.

between crossed polarisers (Fig. 2c). Without polarisers, the texture is uniform suggesting that the aggregation is suppressed (Fig. 2d). Mixtures S_2–S_4 showed a weak aggregation when exposed to the multiple cycles of Iso-LC transition.

At the same time, the current becomes very susceptive to the light. The pronounced photovoltaic effect was observed in the whole range of the LC phase. Fig. 4a shows the photocurrent in S_1 in response to the illumination of various light intensities. The measurements were performed under the bias of 1 V. The current is superimposed with the ionic contribution, which was particularly strong at high temperatures and showed a pronounced time dependence. A slow current decrease with time reflects the development of the space charge double layer. The ionic contribution became small at low temperatures, and the time dependence slowed down. The photocurrent demonstrated only a weak temperature dependence and increased linearly with rising light intensity, as shown in Fig. 4b.

In mixtures with a higher concentration of C61, the temperature dependence of the photocurrent became more pronounced. Fig. 4 shows the photocurrent for the mixtures S_2 and S_3. The photocurrent increases by more than an order of magnitude in the mixture S_3. At the same time, the intensity dependence remained linear in the measured intensity range.

Interestingly, there is a clear dependence of the photocurrent on the concentration of C61 up to 8.7 mol%. This can be attributed to the saturation of the C61 mixtures and the building of aggregates in S_4, resulting in a nearly constant bulk concentration of C61. The dark current, however, did not show any markable dependence on the dopant concentration, and conductivity remained the same for all three mixtures.

The charge mobility was measured with ToF technique using excitation at 532 nm. Fig. 5a shows the typical ToF signal. The signal has a dispersive character. The corresponding mobilities are shown in Fig. 5b.

The mixtures exhibit hole mobilities, which are nearly temperature-independent in the cubic phase suggesting the hopping transfer mechanism. The mobility values are comparable with those of the SmC and SmB phases in typical 2-phenyl naphthalene and terthiophene derivatives.[31] At high temperatures, the mobility starts increasing with increasing temperature. Such an increase of the charge mobility with increasing temperature suggests a temperature-activated distributed density of states responsible for charge transport.

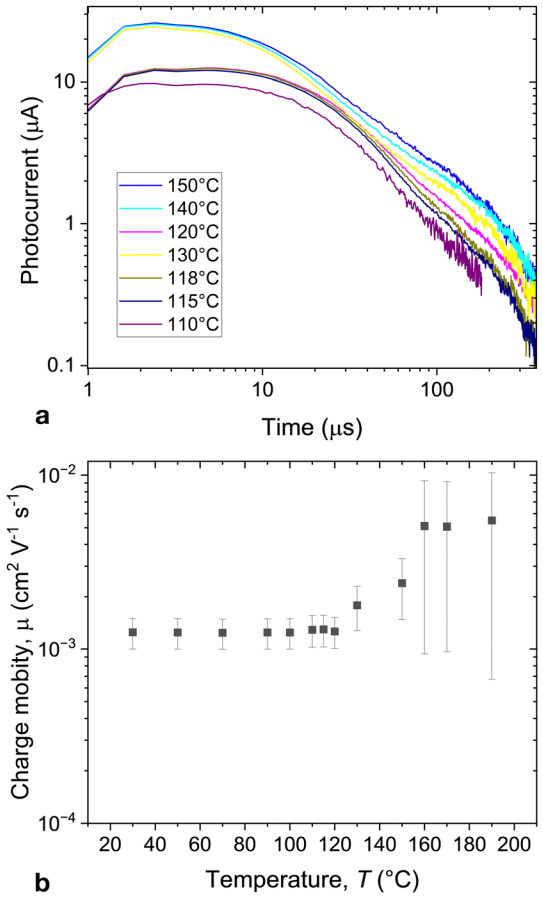

Fig. 5 (a) Photocurrent in time of flight experiments recorded in mixture S_3 at T = 100 °C (dark current subtracted), (b) temperature dependence whole mobilities in S_3.

4 Conclusions

We demonstrated that doping the nanostructured cubic bicontinuous phases of polycatenar mesogens with the electron acceptor fullerene results in a significant enchancement of the photovoltaic effect in the visible spectral range. The photocurrent reaches the values of 160 nA at 8 mV cm^{-2}. At the same time, the pure compound did not show any detectable photovoltaic response. Having the charge mobility comparable with that of SmC and SmB phases of terthiophene derivatives, bicontinuous phases have an advantage over other structures as they don't need any extra alignment, and their charge transport is less affected by structural defects. Unlike 1D and 2D systems, 3D structures offer more options for the charge to find an alternate path to avoid a defective site.

Data availability

The experimental data for this article are included in the presented article.

Conflicts of interest

There are no conflicts to declare.

Acknowledgements

AE thanks Masahiro Funahashi and Fumito Araoka for fruitful discussions. This research was supported by the German Research Foundation (Deutsche Forschungsgemeinschaft, DFG), project ER467/17-1 and AL2378/1-2 (424355983). A. F. Darweesh acknowledges the support by the Alexander von Humboldt Foundation for the research fellowship at Martin

Luther University Halle-Wittenberg, Germany. The authors thank Hajnalka Nádasi for fruitful discussions and preparation of fullerene doped hybrids.

References

1 T. Kato, J. Uchida, T. Ichikawa and T. Sakamoto, *Angew. Chem., Int. Ed.*, 2018, **57**, 4355–4371.
2 W. Pisula, M. Zorn, J. Y. Chang, K. Müllen and R. Zentel, *Macromol. Rapid Commun.*, 2009, **30**, 1179.
3 T. Kato, M. Yoshio, T. Ichikawa, B. Soberats, H. Ohno and M. Funahashi, *Nat. Rev. Mater.*, 2017, **2**, 17001.
4 H. K. Bisoyi and Q. Li, *Prog. Mater. Sci.*, 2019, **104**, 1–52.
5 H. Iino, T. Usui and J.-i Hanna, *Nat. Commun.*, 2015, **6**, 6828.
6 D. H. Kim, B.-L. Lee, H. Moon, H. M. Kang, E. J. Jeong, J.-I. Park, K.-M. Han, S. Lee, B. W. Yoo, B. W. Koo, J. Y. Kim, W. H. Lee, K. Cho, H. A. Becerril and Z. Bao, *J. Am. Chem. Soc.*, 2009, **131**, 6124–6132.
7 O. Kwon, X. Cai, W. Qu, F. Liu, J. Owska, E. Gorecka, M. J. Han, D. K. Yoon, S. Poppe and C. Tschierske, *Adv. Funct. Mater.*, 2021, **31**, 2102271.
8 M. Funahashi, *Mater. Chem. Front.*, 2021, **5**, 8265–8274.
9 C. Dressel, F. Liu, M. Prehm, X. Zeng, G. Ungar and C. Tschierske, *Angew. Chem., Int. Ed.*, 2014, **53**, 13115–13120.
10 Y. Cao, M. Alaasar, A. Nallapaneni, M. Salamończyk, P. Marinko, E. Gorecka, C. Tschierske, F. Liu and N. Vaupotic, *Phys. Rev. Lett.*, 2020, **125**, 027801.
11 X. Zeng and G. Ungar, *J. Mater. Chem. C*, 2020, **8**, 5389–5398.
12 M. Alaasar, S. Poppe, Q. Dong, F. Liu and C. Tschierske, *Angew. Chem.*, 2017, **129**, 10941–10945.
13 M. Alaasar, M. Prehm, Y. Cao, F. Liu and C. Tschierske, *Angew. Chem.*, 2016, **128**, 320–324.
14 Y. Cao, M. Alaasar, L. Zhang, C. Zhu, C. Tschierske and F. Liu, *J. Am. Chem. Soc.*, 2022, **144**, 6936–6945.
15 M. Alaasar, A. F. Darweesh, X. Cai, F. Liu and C. Tschierske, *Chem. – Eur. J.*, 2021, **27**, 14921–14930.
16 C. Dressel, T. Reppe, S. Poppe, M. Prehm, H. Lu, X. Zeng, G. Ungar and C. Tschierske, *Adv. Funct. Mater.*, 2020, **30**, 2004353.
17 J. Matraszek, D. Pociecha, N. Vaupotič, M. Salamończyk, M. Vogrin and E. Gorecka, *Soft Matter*, 2020, **16**, 3882–3885.
18 T. Reppe, S. Poppe, X. Cai, Y. Cao, F. Liu and C. Tschierske, *Chem. Sci.*, 2020, **11**, 5902–5908.
19 T. Reppe, C. Dressel, S. Poppe, A. Eremin and C. Tschierske, *Adv. Opt. Mater.*, 2021, **9**, 2001572.
20 M. Alaasar, Y. Cao, Y. Liu, F. Liu and C. Tschierske, *Chem. – Eur. J.*, 2022, **28**, e202201857.
21 P. Li, Y. Lin, Z. Qi and D. Yan, *J. Mater. Chem. A*, 2023, **11**, 21078–21088.
22 M. A. Mushtaq, A. Kumar, G. Yasin, M. Arif, M. Tabish, S. Ibraheem, X. Cai, W. Ye, X. Fang, A. Saad, J. Zhao, S. Ji and D. Yan, *Appl. Catal., B*, 2022, **317**, 121711.
23 X.-G. Yang, Z.-M. Zhai, X.-M. Lu, L.-F. Ma and D. Yan, *ACS Cent. Sci.*, 2020, **6**, 1169–1178.
24 R. Gao, M. S. Kodaimati and D. Yan, *Chem. Soc. Rev.*, 2021, **50**, 5564–5589.
25 R. Gao, Q. Dai, F. Du, D. Yan and L. Dai, *J. Am. Chem. Soc.*, 2019, **141**, 11658–11666.
26 M. Dai and D. Yan, *Sci. Chin. Chem.*, 2022, **65**, 831–833.
27 T. Yasuda, H. Ooi, J. Morita, Y. Akama, K. Minoura, M. Funahashi, T. Shimomura and T. Kato, *Adv. Funct. Mater.*, 2009, **19**, 411–419.
28 X. Zhang, C. Hsu, X. Ren, Y. Gu, B. Song, H. Sun, S. Yang, E. Chen, Y. Tu, X. Li, X. Yang, Y. Li and X. Zhu, *Angew. Chem., Int. Ed.*, 2015, **54**, 114–117.
29 X. Yang, T. Zhu and Y. Tu, *Full. Liq. Crys.*, 2020, 149–171.
30 Y. Zhang, I. Murtaza and H. Meng, *J. Mater. Chem. C*, 2018, **6**, 3514–3537.
31 T. Kato, M. Yoshio, T. Ichikawa, B. Soberats, H. Ohno and M. Funahashi, *Nat. Rev. Mater.*, 2017, **2**, 17001.